MODELING AND MEASUREMENTS OF THE IMPACT OF DIPOLE FRINGE FIELDS IN THE EXTRA LOW ENERGY ANTIPROTON RING

S. Van der Schueren*[1], R. De Maria, D. Gamba, CERN, Geneva, Switzerland
M. Migliorati, University of Rome La Sapienza, Rome, Italy
[1]also at University of Rome La Sapienza, Rome, Italy

Abstract

The ELENA (Extra Low ENergy Antiproton) ring is a compact synchrotron designed to decelerate antiprotons delivered by the Antiproton Decelerator. In ELENA, the beam dynamics are dominated by the dipole edges, making this machine an ideal tool for benchmarking theoretical fringe field models against direct beam measurements. In this paper, we present a comparison of theoretical models and experimental data to characterize the impact of fringe fields and evaluate the accuracy of existing fringe field descriptions.

INTRODUCTION

Fringe fields have well known and less well known effects on beam dynamics. To investigate which effects are important in small machines, we performed measurements in the ELENA ring [1] at CERN, for which the optics is dominated by the dipole edges.

DIPOLE MODELS

In this paper, we will compare different fringe field models using Xsuite [2]. The currently used Xsuite model is the model described in [3], specified by an edge angle and a fringe field integral. We will compare three different sets of parameters in Xsuite: the *design parameters* as mentioned in [1], the currently used parameters (see Table 1) that are available in the *acc-models* database [4] where the edge angle was optimised based on an OPERA [5] simulation, and a new set of *fitted* parameters where both the edge angle and the fringe field integral were determined based on a fit of the transfer matrix of the dipole fieldmap, using the method explained in the following subsection.

Accurate Modeling

More accurate simulations that will serve as a benchmark for our models will be based on an electromagnetic fieldmap obtained from interpolated measurements using BEM-based magnetic field reconstruction [6]. To describe the fieldmap of the magnet, one can use an expansion in Frenet-Serret coordinates [7],

$$\vec{R}(x,y,s) = \vec{R}_0(s) + x\hat{x}(s) + y\hat{y}(s) \tag{1}$$

$$\frac{d}{ds}\vec{R}_0(s) = \hat{s}(s)\ , \tag{2}$$

with $\vec{R}$ the position of the particle, $\vec{R}_0$ the position of the reference trajectory, and $\hat{x}$ and $\hat{y}$ the horizontal and vertical unit vectors of a coordinate system anchored to the reference trajectory. We have that $\hat{s} = \vec{R}_0'(s)$, $\hat{x}'(s) = h(s)\hat{s}(s)$ and $\hat{y}(s) = -\hat{x}(s) \times \hat{s}(s)$ and $h(s) = 1/\rho(s)$ is the local curvature, see Fig. 1 for the specific case that will be used later. Essentially, we define a frame with a fixed curvature equal to the design value in a region inside the theoretical magnetic length, and zero curvature outside of this region.

Table 1: Sets of Parameters for the Different Fringe Field Models Plugged into Xsuite

Parameter set	θ_E	F_{int}
Design parameters	17°	0.424
Acc-models parameters	16.45°	0.424
Fitted parameters	16.40°	0.399

To specify the magnetic field in the dipole, one can extract the derivatives on axis (on the reference trajectory) from the fieldmap in this frame at every longitudinal position,

$$a_n(s) = \partial_x^{n-1} B_x(x,y,s)\big|_{x=y=0} \tag{3}$$

$$b_n(s) = \partial_x^{n-1} B_y(x,y,s)\big|_{x=y=0} \tag{4}$$

$$b_s(s) = B_s(x=0,y=0,s) \tag{5}$$

from which the total magnetic field can be reconstructed. This can be done by defining initial functions ϕ_0 and ϕ_1 for the magnetic scalar potential,

$$\phi_0(x,s) = -a_0(s) - \sum_{n=1}^{\infty} a_n(s)\frac{x^n}{n!} \tag{6}$$

$$\phi_1(x,s) = -\sum_{n=1}^{\infty} b_n(s)\frac{x^{n-1}}{(n-1)!} \tag{7}$$

such that the complete scalar potential can be determined by

$$\Phi(x,y,s) = \sum_{i=0}^{\infty} \phi_i(x,s)\frac{y^i}{i!}\ , \tag{8}$$

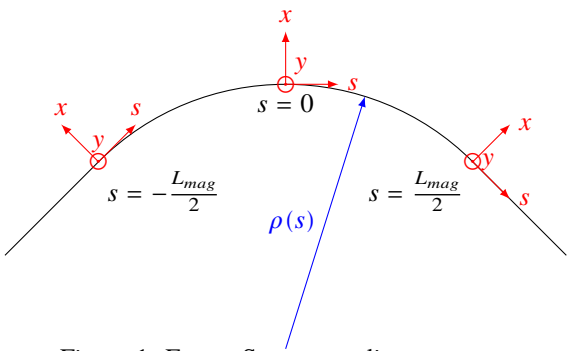

Figure 1: Frenet-Serret coordinate system.

* silke.van.der.schueren@cern.ch

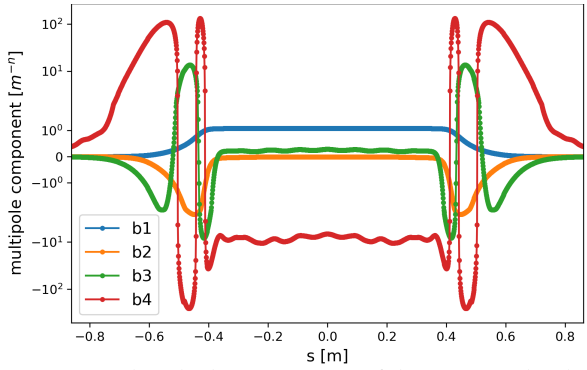

Figure 2: Multipole decomposition of the ELENA dipole up to octupole component. Third order piecewise polynomials are used to describe the longitudinal behaviour. The uncertainty of the fit was estimated by varying the highest order of the fitted polynomial and it was in the order of 0.0002%, 0.07%, 0.8%, 43% of the maximal value for b_1, b_2, b_3, b_4 respectively.

with recursion relation

$$\phi_{i+2} = -\frac{1}{1+hx}\left(\partial_x((1+hx)\partial_x\phi_i) + \partial_s\left(\frac{1}{1+hx}\partial_s\phi_i\right)\right). \quad (9)$$

The magnetic field is then uniquely defined by the scalar potential $\mathbf{B} = -\nabla\Phi$ [8].

The derivatives on axis can be determined from a magnetic fieldmap at a set of discrete longitudinal positions. In our situation, we chose to fit the derivatives through a polynomial fit, to have better noise tolerance than calculating numerical derivatives. However, we noticed that the fitting using this method is highly sensitive to the number of higher-order multipoles included, which leads to large uncertainties. We plan to investigate other options, such radial dependent harmonic analysis and conversion to field derivatives.

To track the particles, one needs a description of the longitudinal behaviour of the functions $a_n(s)$, $b_n(s)$. While the lowest order component of a fringe field, in this case $b_1(s)$, can accurately be described by Enge functions [9], the higher-order components do not allow such easy description. For this reason, a piecewise description with third order polynomials with continuous first-order derivatives was chosen. The decomposition of the magnet in normal multipole components up to octupoles, together with the polynomial fit, is given in Fig. 2.

Once the derivatives on axis are determined, one can then track particles through the fieldmap using a fourth-order Runge-Kutta method [10], solving the Hamilton equations with the Hamiltonian for a particle in an electromagnetic field in Frenet-Serret coordinates,

$$H_\tau = \frac{p_\tau}{\beta_0} - (1+hx) \times \left(\sqrt{(1+\delta)^2 - (p_x - a_x)^2 - (p_y - a_y)^2} + a_s\right). \quad (10)$$

This method will be referred to as *fieldmap tracking*, and was used to determine the fitted parameters in Table 1.

Table 2: Comparison of different tune predictions to measurements, reproducible with a standard deviation of $5\cdot10^{-4}$.

Parameter set	Q_x	Q_y
Design parameters	1.7896	1.7708
Acc-models parameters	1.8362	1.7279
Fitted parameters	1.8406	1.7347
fieldmap tracking	1.8364	1.7386
Measurement	x.8453	x.7386

MEASUREMENT SETUP

The measurements have been performed with a H^--beam, which has similar properties as the antiproton beam. Since the optics of the ELENA machine is dominated by the dipole edges, it is possible to obtain a stable ring without quadrupoles. The advantage of this setup is a very simple lattice in which the effect of the dipoles can be isolated.

The measurements were performed at 5.3 MeV, right after accelerating the beam from the injection energy of 0.1 MeV. To exclude the effects of the Eddy currents, a compensation was added to the dipole currents and the measurements were performed only once a stable situation was reached. To perform the tune measurements, a chirp excitation was applied to the beam. This is a horizontal (vertical) kick with a frequency that is varied around the expected tune from simulation, between 0.83 and 0.86 (0.73 and 0.75). Applying a Fourier transform on the dedicated electrostatic pickup data allows extracting the tune from the measurements. Further, the RF frequency was varied to measure also the chromatic behaviour of the machine.

Tune Measurements

The tune as predicted by the different models is given in Table 2 together with the measurements. When comparing the measurements in the horizontal plane, one can see an improvement in all three optimised models over the design model. Further improvement of the model is needed, although a possible explanation of this measurement could be the spurious horizontal orbit present in the machine, that could not be further corrected at the time of measurement. In the vertical plane, one can see the impact of also optimising the fringe field integral, as was done in our fitted parameter model, obtaining very good agreement with the measurements.

Chromaticity Measurements

A comparison of the measurements as a function of the RF frequency against the different models is given in Fig. 3. The measurements were performed both with and without electron cooler to investigate the non-linear effects of the magnetic fields of the electron cooler on the beam. The difference in horizontal plane could possibly be explained by a difference in horizontal orbit [11].

The deviation from the lumped fringe field map with the measurements is not unexpected, since such a model intro-

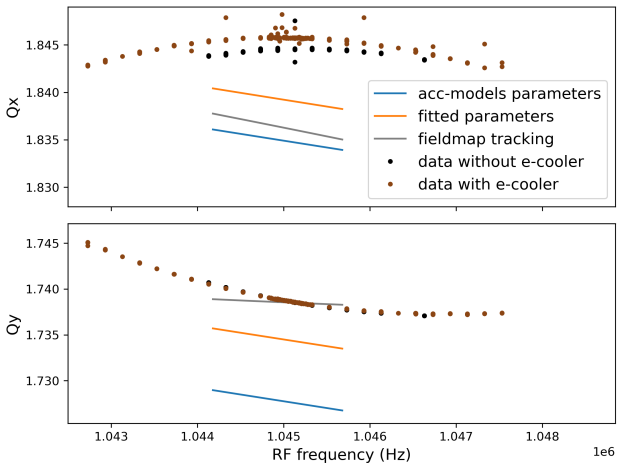

Figure 3: Comparison of the tune measurements as function of frequency for all different models. The data with and without electron cooler overlaps in the lower plot.

duces several simplifications on the non-linear dynamics. To include an accurate description of the sextupolar effect one would need to include the pole face curvature [12], and for the higher order effects and feed-down from the closed orbit distortion, a more advanced fringe field map, such as in [13], could be explored.

When comparing the measurement to the tracking with magnetic fieldmap, one can observe that the linear chromaticity does not agree. Since the horizontal orbit in the machine could not be corrected, and it is also not exactly known due to possible misalignments of the bpms, the same RF frequency can correspond to a different momentum between the models.

Although the value for the non-linear chromaticity does not agree with the measurements, they fall well within the uncertainty on the octupole component of our model. To explain the measurements, one would need an integrated normalized octupole component of -40 m^{-2}, while our integrated octupole field is -3 ± 200 m^{-2}, hence a deviation of only 0.2σ. Improvements to the multipole extraction from fieldmap will be needed to reduce the uncertainties and draw further conclusions.

CONCLUSIONS

In this paper, we compare different parameter sets and models for the ELENA dipoles against measurements of machine observables. We conclude that the linear optics, excluding the effect of the closed orbit, can be well described and accurately predicted by both explicit tracking through a fieldmap and the lumped map available in Xsuite with optimized parameters. To describe the non-linear behaviour of the machine, the lumped map with two parameters is not sufficient and one needs to explore better lumped maps or resort to explicit tracking through the field map. To reach a predictive description of the non-linear behaviour, improved fitting methods to determine the derivatives on axis are needed. One possible more robust solution could be the use of a harmonic analysis of the three dimensional data at multiple radii, similar to that for for s-dependent multipoles in a straight frame [14], after which one can transform the harmonic expansion into derivatives on axis. The advantage of this method would be that the full three-dimensional fieldmap is used, instead of data on the midplane only.

ACKNOWLEDGEMENTS

The authors would like to thank M. Liebsch for providing the field map and interpolation method of the ELENA dipole. We further thank J. Romain and L. Ponce for their assistance with the measurements.

REFERENCES

[1] W. Oelert, "The ELENA Project at CERN", *Acta Phys. Polon. B*, vol. 48, no.10, pp. 1895–1902, 2017. doi:10.5506/APhysPolB.48.1895

[2] G. Iadarola *et al.*, "Xsuite: An integrated beam physics simulation framework", in *Proc. HB'23*, Geneva, Switzerland, Oct. 2023, pp. 73–80. doi:10.18429/JACoW-HB2023-TUA2I1

[3] E. Forest, S. C. Leemann and F. Schmidt, "Fringe effects in MAD part 1: Second-order fringe in MAD-X for the module PTC", KEK, Tsukuba, Japan, Rep. KEK-PREPRINT-2005-109, 2005.

[4] CERN Acc-models database, `https://acc-models.web.cern.ch/acc-models/elena/`

[5] OPERA electromagnetic simulation software, Dassault Sistemes SIMULIA, `https:www.3ds.com/`

[6] M. Liebsch, S. Russenschuck, and S. Kurz, "BEM-based magnetic field reconstruction by ensemble Kálmán filtering", Comp. Meth. Appl. Math., vol. 23, no. 2, pp. 405–424, 2023. doi:10.1515/cmam-2022-0121

[7] E. D. Courant and H. S. Snyder, "Theory of the alternating-gradient synchrotron", *Ann. Phys.*, vol. 281, no. 1–2, pp. 360–408, Apr 2000. doi:10.1006/aphy.2000.6012

[8] S. Van der Schueren, R. De Maria, E. Benedetto, D. Barna, and M. Migliorati, "Magnetic-field modelling and symplectic integration of magnetic fields on curved reference frames for improved synchrotron design: first steps", in *Proc. IPAC'24*, Nashville, TN, USA, May 2024, pp. 1649–1652. doi:10.18429/JACoW-IPAC2024-TUPS09

[9] H. A. Enge, *Focusing of Charged Particles*, New York, NY, USA: Academic Press, 1967. doi:10.1016/B978-0-12-636901-4.X5001-9

[10] J. D. Lambert, *Numerical Methods for Ordinary Differential Systems: The Initial Value Problem*, Hoboken, New Jersey, USA: John Wiley & Sons, 1991. doi:10.2307/2153266

[11] L. Bojtár, "Frequency analysis and dynamic aperture studies in a low energy antiproton ring with realistic 3D magnetic fields", *Phys. Rev. Accel. Beams*, vol. 23, no. 10, p. 104002, 2020. doi:10.1103/PhysRevAccelBeams.23.104002

[12] E. Forest, S. C. Leemann, and S. Schmidt, "Fringe effects in MAD Part 2: Bend curvature in MAD-X for the module PTC", KEK, Tsukuba, Japan, Rep. KEK-PREPRINT-2005-110, 2006.

[13] K. Hwang and S. Y. Lee, "Dipole fringe field thin map for compact synchrotrons", *Phys. Rev. Spec. Top. Accel. Beams*, vol. 18, no. 12, p. 122401, 2015. doi:10.1103/PhysRevSTAB.18.122401

[14] E. Forest, *Beam Dynamics, A New Attitude And Framework*, 1st edition, Boca Raton, FL, USA: CRC Press, 1998.